Mineralogical Magazine, 2014, Vol. 78(2), pp. 293–310

Crystal-chemistry and short-range order of fluoro-edenite and fluoro-pargasite: a combined X-ray diffraction and FTIR spectroscopic approach

G. Della Ventura[1,2,*], F. Bellatreccia[1,2], F. Cámara[3,4] and R. Oberti[5]

[1] Dipartimento di Scienze, Università di Roma Tre, Largo S. Leonardo Murialdo 1, I-00146 Rome, Italy
[2] INFN, Laboratori Nazionali di Frascati, Via E. Fermi, 40, 00044 Frascati, Rome, Italy
[3] Dipartimento di Scienze della Terra, via Valperga Caluso 35, I-10125 Turin, Italy
[4] CrisDi, Interdepartmental Centre for Crystallography, Via P. Giuria 5, 10125, Turin, Italy
[5] CNR-Istituto di Geoscienze e Georisorse, UOS Pavia, via Ferrata 1, I-27100 Pavia, Italy

[*Received 12 December 2013; Accepted 15 December 2013; Associate Editor: S.J. Mills*]

ABSTRACT

This study addresses the crystal chemistry of a set of five samples of F-rich amphiboles from the Franklin marble (USA), using a combination of microchemical (Electron microprobe analysis (EMPA)), single-crystal refinement (SREF) and Fourier transform infrared (FTIR) spectroscopy methods. The EMPA data show that three samples fall into the compositional field of fluoro-edenite (Hawthorne *et al*., 2012), whereas two samples are enriched in high-charged C cations and – although very close to the $^{C}R^{3+}$ boundary – must be classified as fluoro-pargasite. Magnesium is by far the dominant C cation, Ca is the dominant B cation (with ^{B}Na in the range 0.00−0.05 a.p.f.u., atoms per formula unit) and Na is the dominant A cation, with $^{A}\square$ (vacancy) in the range 0.07−0.21 a.p.f.u.; ^{W}F is in the range 1.18−1.46 a.p.f.u. SREF data show that: ^{T}Al is completely ordered at the *T*(1) site; the *M*(1) site is occupied only by divalent cations (Mg and Fe^{2+}); ^{C}Al is disordered between the *M*(2) and *M*(3) sites; ^{A}Na is ordered at the *A*(*m*) site, as expected in F-rich compositions. The FTIR spectra show a triplet of intense and sharp components at ~3690, 3675 and 3660 cm^{-1}, which are assigned to the amphibole and the systematic presence of two very broad absorptions at 3560 and 3430 cm^{-1}. These latter are assigned, on the basis of polarized measurements and FPA (focal plane array) imaging, to chlorite-type inclusions within the amphibole matrix. Up to eight components can be fitted to the spectra; band assignment based on previous literature on similar compositions shows that ^{C}Al is disordered over the *M*(2) and *M*(3) sites, thus supporting the SREF conclusions based on the <*M*−O> bond distance analysis. The measured frequencies of all components are typical of O−H groups pointing towards Si−O(7)−Al tetrahedral linkages, thus allowing characterization of the SRO (short-range-order) of ^{T}Al in the double chain. Accordingly, the spectra show that in the fluoro-edenite/pargasite structure, the T cations, Si and Al, are ordered in such a way that Si−O(7)−Si linkages regularly alternate with Si−O(7)−Al linkages along the double chain.

Keywords: fluoro-edenite, fluoro-pargasite, EMPA, single-crystal structure refinement, FTIR powder and single-crystal spectra, FPA imaging, short-range order.

* E-mail: giancarlo.dellaventura@uniroma3.it
DOI: 10.1180/minmag.2014.078.2.05

This paper is published as part of a special issue of *Mineralogical Magazine*, Volume **78(2)**, 2014, in celebration of the International Year of Crystallography.

Introduction

EDENITE, ideally $NaCa_2Mg_5(Si_7Al)O_{22}(OH)_2$, is an endmember of the Ca amphibole subgroup (Hawthorne *et al.*, 2012) and hence an hydroxyl-bearing double-chain silicate. It was first described by A. Breithaupt in 1874 based on a specimen from Franklin Furnace, New Jersey, USA (Clark, 1993). However, neither that sample nor the one studied later by Palache (1935) from the Franklin marble falls within the compositional range of edenite, as defined by the succeeding International Mineralogical Association Subcommittees on Amphiboles, i.e. then $^{B}Ca \geqslant 1.50$ a.p.f.u. (atoms per formula unit), $^{A}(Na,K) \geqslant 0.50$ a.p.f.u., $7.50 < {}^{T}Si < 6.50$ a.p.f.u. and presently $^{W}(OH,F)$ and ^{A}Na dominant, $^{B}Ca/^{B}(Ca+Na) \geqslant 0.75$, $0.00 < {}^{C}R^{3+} \leqslant 0.50$ (e.g. Hawthorne *et al*., 2012). In fact, re-examination of several samples from the marble quarries in the Franklin area, kept and labelled as edenite in various Mineralogical Museums all around the world, has shown these to be pargasite, or edenitic magniesio-hornblende or pargasitic-hornblende (our unpublished work; M. Lupulescu, pers. comm.)

Several attempts have been made to grow edenite experimentally. However, in OH-bearing systems the synthesis of endmember edenite has never been successful (Gilbert *et al.*, 1982). Na *et al.* (1986) investigated the phase relations in the system edenite + H_2O and edenite + excess quartz + H_2O. They found that, when quartz is not in excess, phlogopite is the stable phase over a wide range of conditions including the amphibole *P-T* field, thus suggesting that edenite is probably stable only under very high a_{SiO_2}. Indeed, excess quartz in the system stabilizes the amphibole; however, the compositions obtained are systematically solid-solutions in the ternary system tremolite–richterite–edenite. Della Ventura and Robert (unpublished data) failed to synthesize edenite at T = 700ºC and P_{H_2O} = 1 kbar. Della Ventura *et al.* (1999) studied the richterite–pargasite join and observed that the amphibole is substituted by a Na-rich mica when approaching the edenite stoichiometry. In contrast, fluoro-edenite has been obtained easily by several authors in OH-free systems. Kohn and Comeforo (1955) synthesized fluoro-edenite and B-rich fluoro-edenite starting from a mixture of oxides, at P = 1 atm and using the melting technique, with slow cooling from 1350ºC. The wet-chemical analysis of the bulk run-product gave: $Na_{0.99}(Ca_{1.84}Na_{0.16})(Mg_{4.79}Al_{0.18})(Si_{7.12}Al_{0.88})O_{22}F_{2.15}$. Graham and Navrotsky (1986) obtained high-yield amphibole run products, with <5% pyroxene impurities along the fluoro-tremolite–fluoro-edenite join. Raudsepp *et al*. (1991) also failed to synthesize edenite in the OH-system, but obtained high fluoro-edenite yields (>90%) at P = 1 atm; in their case, EMPA showed significant deviation towards tschermakite. Boschmann *et al.* (1994) synthesized fluoro-edenite (with ^{B}Mg contents close to 0.20 a.p.f.u.) using the same technique (slow cooling from 1240ºC) and characterized their product by X-ray single-crystal diffraction and EMPA. The crystals were strongly zoned, from a core with composition close to endmember fluoro-edenite to a rim with composition intermediate between fluoro-tremolite and fluoro-pargasite. X-ray single-crystal refinement (SREF) showed that ^{T}Al is strongly ordered at $T(1)$ and suggested that ^{C}Al is strongly ordered at $M(2)$, the latter being a conclusion that should be revised in the light of this work. Gianfagna and Oberti (2001) reported on the occurrence of fluoro-edenite very close to the ideal composition, $NaCa_2Mg_5Si_7AlO_{22}F_2$, within the cavities of an altered benmoreitic lava at Biancavilla (Catania, Italy). Oberti *et al.* (1997) characterized a synthetic Mn-rich fluoro-edenite $[Na_{1.06}(Ca_{1.41}Na_{0.12}Mn_{0.47})(Mg_{4.44}Mn_{0.41}Al_{0.15})(Si_{6.91}Al_{1.09})O_{22}F_{2.00}]$ and commented on Mn^{2+} partitioning. Later, Oberti *et al.* (2006) reported on the occurrence of $^{A}(Na_{0.74}K_{0.02})\,{}^{B}(Ca_{1.27}Mn_{0.73})\,{}^{C}(Mg_{4.51}Mn^{2+}_{0.28}Fe^{2+}_{0.05}Fe^{3+}_{0.03}Al_{0.12}Ti_{0.01})\,{}^{T}(Si_{7.07}Al_{0.93})O_{22}(OH)_2$ – at that time the new endmember parvo-mangano-edenite but now simply ^{B}Mn-rich edenite after Hawthorne *et al*. (2012) – in the Grenville Marble of the Arnold mine, Fowler, St. Lawrence Co., New York (USA). They examined the possible bond-valence configurations proposed for edenite by Hawthorne (1997) and showed that the presence of ^{B}Mn substituting for ^{B}Ca helps to stabilize the charge arrangement of edenite.

In summary, the rarity of natural amphiboles with the edenite composition, their constant enrichment in Fe or Mn and the failure in obtaining synthetic analogues of edenite, suggest that this amphibole is probably not stable (Raudsepp *et al.*, 1991) as confirmed by bond-valence considerations (Hawthorne, 1997).

Systematic work was undertaken here aimed at obtaining new structural and crystal-chemical data on edenite and fluoro-edenite; this study is

focused on selected fluoro-edenite and fluoro-pargasite samples from the Franklin marble obtained from various mineral collections. A multi-methodological approach was used, which includes EMPA, single-crystal X-ray diffraction and refinement and FTIR spectroscopy. In the last two decades, FTIR spectroscopy in the OH-stretching region has been used extensively in the study of hydrous minerals (e.g. Libowitzky and Beran, 2004 and references therein) and proved to be a fundamental tool for characterizing short-range order/disorder features in amphiboles (Hawthorne and Della Ventura, 2007). In this paper, FTIR spectroscopy also allowed us to address two poorly explored issues in amphibole crystal-chemistry, namely the SRO of Mg/Al at the $M(1-3)$ sites in the ribbon of octahedra and of Si/Al at the $T(1,2)$ sites in the double chain of tetrahedra.

Samples studied

Table 1 lists the labels and localities for the samples studied. All amphiboles, except FK-1, which has been provided as an isolated crystal about 3 cm × 3 cm in size, were extracted manually from the host marble, where the amphibole is associated with calcite, phlogopite- and humite-group minerals. Fluoro-edenite and fluoro-pargasite generally occur as well developed crystals with a prismatic habit along *c* and a colour ranging from grey-green to greenish-brown. The maximum crystal size is ~1 cm along *c*.

Chemical composition

Wavelength dispersive analysis was undertaken using a Cameca SX50 at the CNR Istituto di Geologia Ambientale e Geoingegneria (IGAG), c/o Università di Roma La Sapienza. Analytical conditions were 15 kV accelerating voltage and 15 nA beam current, with a 5 μm beam diameter. Counting time was 20 s on both peak and background. The standards used were: wollastonite (Si*K*α, TAP; Ca *K*α, PET), periclase (Mg*K*α, TAP), corundum (Al*K*α TAP), orthoclase (K*K*α, PET), jadeite (Na*K*α, TAP), magnetite (Fe*K*α, LIF), rutile (Ti*K*α, LIF), Mn, Zn and Cr metal (Mn*K*α, Zn*K*α, LIF; Cr*K*α PET), synthetic fluoro-phlogopite (F*K*α, TAP) and sylvite (Cl*K*α, PET). Analytical errors are 1% rel. Data reduction was performed with the *PAP* method (Pouchou and Pichoir, 1985).

The crystal-chemical formulae were calculated based on 24 (O,OH,F,Cl) and 2 (OH,F,Cl) a.p.f.u., as suggested by the structure refinement which excluded the presence of a significant oxo component ($^{W}O^{2-}$). The final data are given in Table 2. Three samples (G2552, GE408 and G405) fall into the fluoro-edenite compositional field, defined by $0.0 < {}^{C}R^{3+} < 0.5$ a.p.f.u. (Hawthorne *et al.*, 2012), whereas samples J9698 and FK-1 are enriched in high-charged cations at C and hence – although very close to the $^{C}R^{3+}$ boundary – must be classified as fluoro-pargasite. Magnesium is by far the dominant C cation, with minor Fe and Al and very minor Ti. Calcium is the dominant B cation, ^{B}Na being negligible (max 0.05 a.p.f.u. in sample C2552, Table 2). Sodium is the dominant A cation, K being always lower than 0.2 a.p.f.u. and with vacancies ranging from 0.07 to 0.21 a.p.f.u. (Table 2).

Single-crystal structure refinement (SREF)

The studied crystals were selected from mineral separates, mounted on a Philips PW-1100 four-circle diffractometer and examined with graphite-

TABLE 1. Labels and localities for the samples used in this work.

Sample	Occurrence	Name	IGG code
J9698	Edenville, Orange Co., New York, USA; SI	Fluoro-pargasite	1073
C2552	Sterling Hill, Ogdensburg, New Jersey, USA; SI	Fluoro-edenite	1069
GE408	Limecrest-Southdown Quarry, Sparta, New Jersey, USA; FM	Fluoro-edenite	1070
G405	Franklin Quarry, Franklin, New Jersey, USA; FM	Fluoro-edenite	1071
FK1	Edenville, Orange Co., New York, USA; FM	Fluoro-pargasite	1072

SI: Smithsonian Institution; FM: Franklin Mineral Museum

TABLE 2. Microchemical data and crystal-chemical formulae for the samples used in the present work.

	J9698 4 an.	C2552 5 an.	GE408 3 an.	G405 6 an.	FK1 3 an.
SiO_2	47.42	47.83	50.23	48.37	46.59
TiO_2	0.52	0.38	0.07	0.09	0.38
Al_2O_3	11.34	7.29	5.81	9.40	11.14
Cr_2O_3	0.03	0.03	0.03	0.03	0.02
FeO	1.83	4.10	1.51	1.69	3.10
Fe_2O_3	0.00	0.45	0.00	0.00	0.05
MnO	0.03	0.09	0.08	0.02	0.02
MgO	20.26	20.30	22.57	20.90	19.37
ZnO	0.01	0.05	0.03	0.05	0.11
CaO	13.48	12.51	13.36	13.09	13.15
Na_2O	2.95	3.33	2.37	2.69	2.76
K_2O	0.64	0.28	0.61	1.11	0.72
F	3.20	2.89	2.55	3.29	2.63
Cl	0.04	0.05	0.03	0.03	0.11
H_2O^*	0.63	0.71	0.91	0.57	0.85
	102.38	100.29	100.16	101.34	100.98
O=F,Cl	−1.36	−1.23	−1.08	−1.39	−1.13
Total	101.02	99.06	99.08	99.94	99.85
Si	6.60	6.86	7.09	6.80	6.60
Al	1.40	1.14	0.91	1.20	1.40
ΣT	8.00	8.00	8.00	8.00	8.00
Al	0.46	0.09	0.06	0.36	0.46
Fe^{3+}	0.00	0.05	0.00	0.00	0.00
Cr	0.00	0.00	0.00	0.00	0.00
Ti	0.05	0.04	0.01	0.01	0.04
Zn	0.00	0.01	0.00	0.01	0.01
Mg	4.21	4.34	4.75	4.38	4.09
Fe^{2+}	0.21	0.49	0.18	0.20	0.37
Mn^{2+}	0.00	0.01	0.01	0.00	0.00
ΣC	4.94	5.03	5.01	4.97	4.98
ΣC	–	0.03	0.01	–	–
Ca	2.00	1.92	1.99	1.97	2.00
Na	0.00	0.05	0.00	0.03	0.00
ΣB	2.00	2.00	2.00	2.00	2.00
Ca	0.01	0.00	0.03	0.00	0.00
Na	0.80	0.88	0.65	0.71	0.75
K	0.11	0.05	0.11	0.20	0.13
ΣA	0.92	0.93	0.79	0.91	0.88
OH	0.58	0.68	0.86	0.53	0.80
F	1.41	1.31	1.14	1.46	1.18
Cl	0.01	0.01	0.01	0.01	0.03
ΣW	2.00	2.00	2.00	2.00	2.00

* calculated; formula normalized to 22 oxygen atoms and 2 (OH,F,Cl).

monochromatized Mo$K\alpha$ X-radiation; crystal quality was assessed *via* profile analysis of Bragg diffraction peaks. Unit-cell dimensions were calculated from least-squares refinement of the *d* values obtained from 50 rows of the reciprocal lattice by measuring the gravity centroid of each reflection and its corresponding antireflection in the θ range −30º to 30º.

Intensity data were collected in the range $2º < \theta < 30º$. Only the monoclinic pairs *hkl* and $h\bar{k}l$ were collected with the Philips PW1100 point detector. Intensities (*I*) were corrected for absorption, Lorentz and polarization effects and then averaged and reduced to structure factors (*F*).

Reflections with $I > 3\ \sigma_I$ were considered as observed during unweighted full-matrix least-squares refinement on *F*. Scattering curves for fully ionized chemical species were used at those sites where chemical substitutions occur; neutral *vs.* ionized scattering curves were used at the *T* and anion sites (except O(3)). Selected crystal data and refinement information are given in Table 3, selected bond distances and site-scattering values are given in Table 4 and refined values of the atomic coordinates and displacement factors are given in Table 5 (which has been deposited with the Principal Editor of *Mineralogical Magazine* and is available from www.minersoc. org/pages/e_journals/dep_mat_mm.html)

Inspection of these data show that: (1) ^{T}Al is completely ordered at the *T*(1) site; (2) only two samples – C2552 and GE408 – show minimal contents of C-type cations as B cations (at the *M*(4′) site); (3) the A cations tend to order at the *A*(*m*) site, as expected in F-rich compositions; (4) the *M*(1) site is only occupied by divalent cations (Mg and Fe^{2+}); (5) the <*M*(3)−O> distances are always shorter than the <*M*(1)−O> distances and in three samples: C2552, GE408 and G405, even shorter than those of the *M*(2) site, where high-charged cations are ordered in (OH,F)-dominant amphiboles. However, the presence of fluorine is known to shorten the <*M*(1)−O> and <*M*(3)−O> distances equally in amphiboles and thus these results are compatible with ^{C}Al disorder between the *M*(2) and *M*(3) sites, which had previously been found only in high *Mg#* [Mg number = $Mg/(Mg+Fe^{2+})$] pargasite crystallized at high *T*, *P* conditions (Oberti *et al.*, 1995*a*). This issue prompted confirmation with an independent technique, such as FTIR spectroscopy, which could also help to identify other peculiarities of local order in fluoro-edenites, and perhaps shed further light on the reasons for the rarity of edenitic compositions. It is useful to recall here that a value of <*M*(3)−O> shorter than <*M*(1)−O> had also been observed in nearly stoichiometric

TABLE 3. Unit-cell dimensions and crystal-structure refinement information.

Sample	J9698	C2552	GE408	G405	FK1-2
a (Å)	9.849(2)	9.865(4)	9.871(3)	9.866(4)	9.862(2)
b (Å)	17.973(4)	18.026(7)	18.033(9)	17.987(11)	17.998(5)
c (Å)	5.2867(14)	5.2836(16)	5.2805(18)	5.2817(25)	5.2942(17)
β (º)	105.17(2)	105.013(24)	104.97(3)	105.16(4)	105.17(2)
V (Å^3)	903.26	907.50	908.02	904.65	906.95
F_{all}	1498	1501	1499	1492	1375
F_{obs} $I > 3\sigma_I$	1346	1342	1326	1325	1212
R_{sym}	1.80	1.10	1.20	1.60	4.30
R_{obs} $I > 3\sigma_I$	1.84	1.42	1.29	1.46	1.77
R_{all}	2.34	1.88	1.68	1.90	1.69
Size (mm)	0.73 × 0.50 × 0.50	0.63 × 0.36 × 0.36	0.51 × 0.30 × 0.26	0.66 × 0.53 × 0.50	0.38 × 0.33 × 0.23
θ-range	2−30º	2−30º	2−30º	2−30º	2−30º
kV	40	50	50	40	50
mA	20	25	20	20	30

TABLE 4. Selected geometrical parameters (Å) and refined site-scattering values (ss, electrns per formula unit).

Sample	J9698	C2552	GE408	G405	FK1-2
<*M*(1)–O>	2.068	2.070	2.069	2.067	2.075
<*M*(2)–O>	2.051	2.077	2.079	2.061	2.054
<*M*(3)–O>	2.055	2.055	2.056	2.054	2.061
<*M*(4)–O>	2.490	2.502	2.505	2.496	2.493
<*A*–O>	2.927	2.923	2.931	2.932	2.934
<*A*(*m*)–O>	2.873	2.862	2.870	2.879	2.882
<*A*(2)–O>	2.630	2.614	2.630	2.641	2.632
<*T*(1)–O>	1.660	1.653	1.646	1.654	1.662
<*T*(2)–O>	1.634	1.632	1.633	1.633	1.634
ss *M*(1)	25.01	25.82	24.52	24.75	25.75
ss *M*(2)	26.79	28.56	25.22	25.97	27.38
ss *M*(3)	12.63	12.93	12.26	12.46	13.03
ss *M*(4)	40.09	39.04	39.53	39.92	40.06
ss *M*(4′)	–	0.90	0.59	–	–
ss *A*	2.37	2.04	1.74	2.68	2.47
ss *A*(*m*)	5.43	5.12	4.68	5.51	5.26
ss *A*(2)	3.12	2.76	2.40	2.71	2.35

fluoro-edenite from Biancavilla (Gianfagna and Oberti, 2001) as well as in the synthetic sample by Boschmann *et al*. (1994). In those cases, however, the absence of OH-stretching bands and hence the impracticability of FTIR analysis did not allow the authors to address and clarify the issue of ^{C}Al ordering.

Powder infrared spectra

The FTIR spectra on powdered samples were collected using a Nicolet Magna 760 spectrophotometer equipped with a KBr beam-splitter and a DTGS detector. The spectra were acquired in the range 4000–400 cm^{-1}, the nominal resolution was 4 cm^{-1} and the final spectra are the average of 32 scans. Samples were prepared as KBr pellets by mixing 7 mg of the powdered samples with 150 mg of KBr. In order to minimize interfering moisture in the pellets, the mineral + KBr powders were dried at 110ºC for 48 h and then pressed at ~9 ton/cm^2 for 5 min. All disks were kept in an oven (110ºC) for 48 h and analysed at room temperature.

The collected spectra consist of a triplet of sharp and intense bands at ~3690, 3675 and 3660 cm^{-1}, respectively (Fig. 1). A minor absorption at ~3640 cm^{-1} is also visible in sample GE408. Although great care was exerted during the sample preparation, a very broad

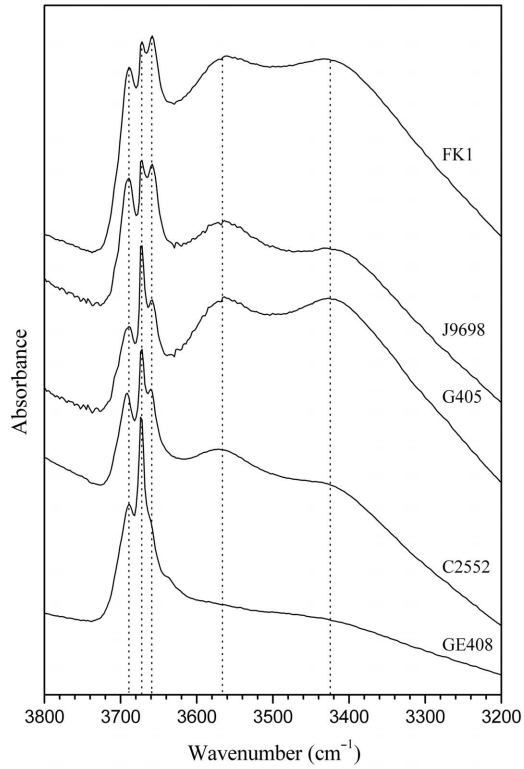

FIG. 1. Infrared OH-stretching powder spectra for the fluoro-amphiboles studied.

absorption in the H_2O region, extending from 3650 to 3000 cm^{-1} is clearly observed in all spectra (Fig. 1). This absorption consists of at least two broad components at 3560 and 3430 cm^{-1}, respectively (Fig. 1). Attempts were made to remove such a broad absorption with repeated heating of the pellets and immediate collection of the spectra; however, only a minor decrease in intensity of this absorption was observed. We had to conclude therefore that the 3560–3430 cm^{-1} components are a real feature of the spectra and are not due to moisture adsorbed on the disk. This point will be discussed below.

Single-crystal infrared spectra and focal plane array (FPA) imaging

Single-crystal spectra were collected with a beam size of 100 μm on randomly oriented double-polished slabs, using a Nicplan IR microscope equipped with a nitrogen-cooled MCT (mercury-cadmium-telluride) detector. 128 scans were averaged for every spectrum; the nominal resolution is 4 cm^{-1}. Several spectra showed the 3560–3430 cm^{-1} broad bands already observed in powder spectra; however, the intensity of these components was extremely variable among the crystals. Representative single-crystal FTIR spectra are displayed in Fig. 2, and are selected to show, for each sample, the less intense absorption at <3600 cm^{-1}. Notably, the broad absorption at 3560–3430 cm^{-1} appears not only in the turbid region of the crystal, but occasionally in the optically clear parts as well. This point is shown in Fig. 3, where several spectra collected in different crystal areas are shown; note that the size of the analysed point is proportional to the beam size. A comparison with Fig. 1 shows that the patterns are very similar to those collected using KBr pellets; in particular, the same triplet of sharp bands at ~3690, 3675 and 3660 cm^{-1} is observed, but the overall intensity of the broad absorptions at 3560–3430 cm^{-1} is greatly reduced. From these observations we conclude that the triplet of sharp bands is due to the amphibole phase, while the 3560–3430 cm^{-1} bands must be assigned to inclusions.

To identify the nature of the inclusions, polarized spectra were first collected on some grains (using a gold wire grid on a ZnSe substrate IR polarizer) and all bands, including the amphibole triplet and the two additional broad absorptions were observed to have variable intensity as a function of the orientation of the electrical vector **E** with respect to the crystals. These measurements were undertaken on randomly oriented samples and thus do not allow any conclusions concerning the orientation of the O–H absorber in the mineral. However, they preclude the assignment of the broad absorptions at <3600 cm^{-1} to randomly oriented fluid or solid inclusions and rather suggest the presence of some extra phase with a specific crystallographic orientation within the amphibole matrix. With the aid of literature data on hydrated substances (e.g. Farmer, 1974), this extra phase was identified as a chlorite-type phyllosilicate. Selected single-crystal slices were studied using a Bruker Hyperion 3000 FTIR microscope equipped with a 64×64 FPA of detectors and a $\times 15$ Cassegrain objective at the INFN Laboratory of Frascati (Rome). The nominal resolution was 8 cm^{-1} and 128 scans were

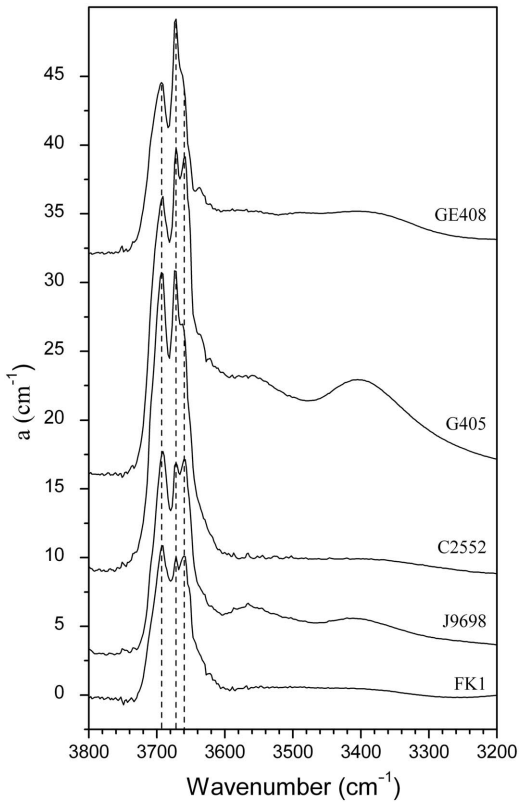

FIG. 2. Single-crystal infrared OH-stretching spectra for the fluoro-amphiboles studied. Absorbance scale normalized to thickness.

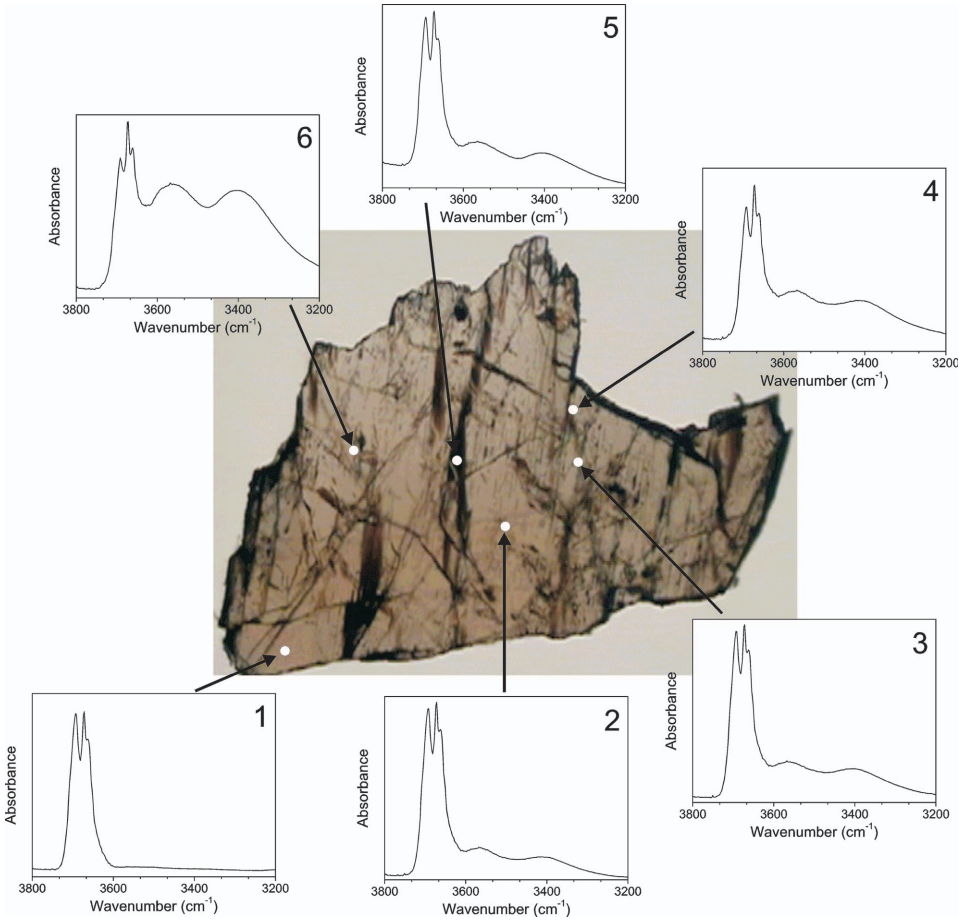

FIG. 3. Variation of the OH-stretching spectrum as a function of the point analysed. Sample C2552, thickness 174 μm.

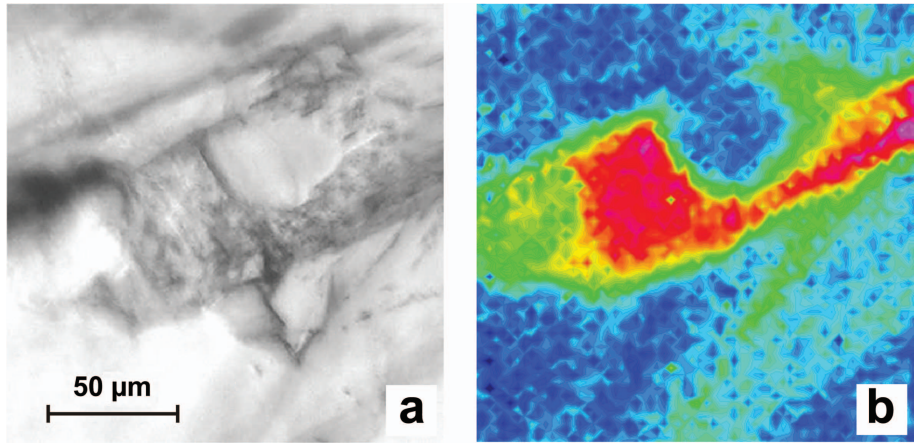

FIG. 4. (*a*) Selected optical image of sample C2552; (*b*) corresponding FPA image. The scale colour from blue (minimum) to red (maximum) is proportional to the intensity in the water stretching 3720−3200 cm^{-1} region.

averaged for the final spectra. Figure 4 shows the image obtained at point 6 in Fig. 3 by integrating the intensity in the whole 3720−3200 cm^{-1} frequency range. It shows the presence of a highly hydrated phase within the fluoro-edenite host, which corresponds to the intermixed layer silicate identified above. Optical observations show that this phase is typically oriented along the cleavage planes of the amphibole. The FTIR spectra show that the phyllosilicate has an absorption in the integrated range which is far greater than in the fluoro-edenite matrix; this suggests that, while the host amphibole is F-rich (see above), the associated layer-silicate is OH-rich, indicating that the hydroxyl component has a strong preference for the layer-silicate structure with respect to the edenite structure. Kock-Muller *et al*. (2004) observed a similar feature in the spectra of omphacitic clinopyroxenes of mantle origin from beneath the Siberian platform and could assign them, using FTIR and analytical transmission electron microscopy (TEM), to micrometric-to-nanometric chlorite-type and amesite inclusions. Note that TEM data collected on chips extracted from several zones of the pyroxene crystals showed that these guest phyllosilicates were present in both inclusion-rich and optically clear parts of the pyroxenes (Kock-Muller *et al.*, 2004). Similar intergrowths were observed by Cámara (1995) at the TEM scale on samples of amphibole in metabasites from the Nevado-Filabride complex. Analytical electron microscopy showed that the amphibole has compositions related to edenite with significant glaucophane components and hosts chlorite-biotite-quartz intergrowths at the nanoscale. Similar alteration textures were described in micaschists from the same complex by Soto (1991), consisting of chlorite+paragonite retrograde alteration developing in fractures in ferro-glaucophane.

Spectrum fitting and band assignments

The digitized spectra of Fig. 2 were fitted by interactive optimization followed by least-squares refinement (Della Ventura *et al*., 1996); the background was treated as linear and all bands were modelled as symmetric Gaussians (Strens, 1974). The spectra were fitted to the smallest number of peaks needed for an accurate description of the spectral profile. The distribution of absorption, y, as a function of energy (wavenumber, x) was described by the relation $y = A \exp [-0.5 (x - P/W)^2]$ where A is the amplitude, P is the peak centroid and W is the full-width at half-maximum height (FWHM). The spectral parameters (position and width) of some strongly overlapping peaks were refined where these peaks are most prominent and then fixed

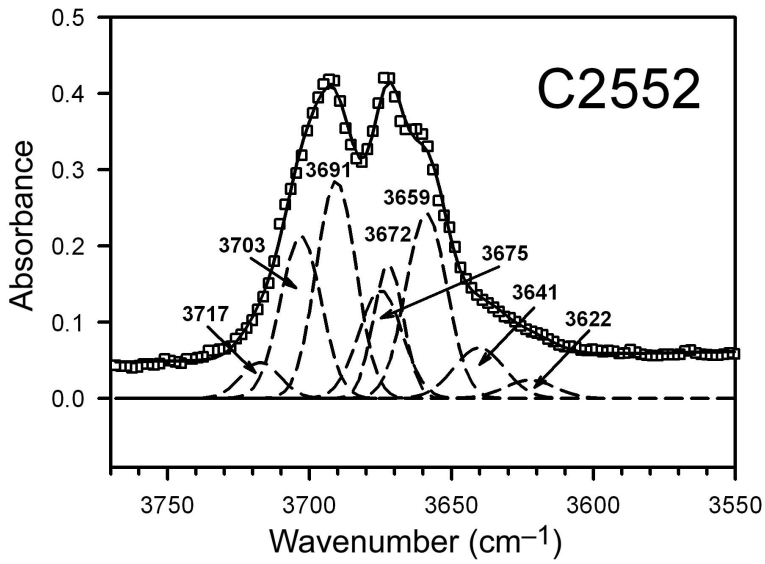

FIG. 5. The fitted spectrum of sample C2552; open squares: experimental pattern, broken lines: fitted bands, line: resulting envelope.

during the refinement of the other samples. This is clearly the case of the tremolite band at ~3670 cm^{-1} (band T in Fig. 6) that was refined in samples G405 and G408 and then added to all other samples on the basis of the EMPA + XRD results which indicated a systematic presence of $^{A}\square$ in the structures of the specimens examined. At convergence, the peak positions were released and only the FWHM were constrained to be roughly constant in all spectra.

A typical example of a fitted spectrum is shown in Fig. 5, while all the relevant data are given in Table 6. The spectra of the samples studied consist of two doublets at 3703−3691 and 3675−3659 cm^{-1} having similar relative intensity and frequency separation (~15 cm^{-1}), a sharp band at ~3672 cm^{-1} and two rather broad bands at 3641−3622 cm^{-1} which account for the tails of the absorption.

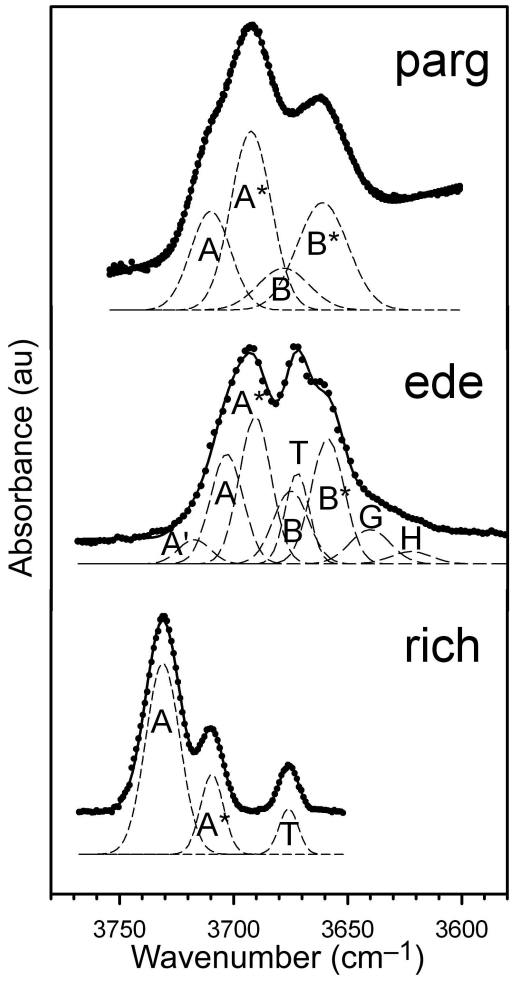

FIG. 6. The fitted spectrum of Fig. 5 (middle) compared with the fitted spectra of synthetic fluoro-pargasite (top, from Robert *et al*., 2000) and synthetic fluoro-richterite (bottom, from Robert *et al*., 1999), both the synthetic samples samples having F = 1.2 a.p.f.u.

Assignment of these bands can be based on previous studies of synthetic (OH,F) amphiboles; the spectrum of fluoro-edenite C2552 (this work) is compared in Fig. 6 with the spectra of a fluoro-pargasite from Robert *et al.* (2000) and a fluoro-richterite from Robert *et al.* (1999), both of which have F = 1.2 and OH = 0.8 a.p.f.u.

The spectrum of synthetic fluoro-richterite (Fig. 6, bottom) shows a main band (A) at 3730 cm^{-1} which is assigned to an O−H group bonded to a $^{M(1)}Mg^{M(1)}Mg^{M(3)}Mg$ trimer of octahedra (Robert *et al*., 1989; Della Ventura, 1992; Robert *et al.*, 1999), directed parallel to *a** and pointing toward ^{A}Na when the A cavity is built by a ring of tetrahedra all occupied by Si. This configuration can be expressed as MgMgMg–OH–^{A}Na:SiSi when using the notation of Della Ventura *et al*. (1999) and Hawthorne *et al.* (2000). While OH is replaced by F, a new band appears in the spectrum at 3710 cm^{-1} (A*); its position does not depend on the OH/F ratio and its relative intensity varies with the F content. The reason for the observed downward shift of the OH-band due to the $OH_{-1}F$ substitution has been discussed in detail by Robert *et al.* (1999). It is based on the observation that in F-rich amphiboles the A cation is displaced from the centre of the cavity, along the mirror plane and towards the fluorine site (i.e. at the *A*(*m*) site), in agreement with the presence of *A*–F attraction (Hawthorne *et al.*, 1996*a*). This shift reduces the repulsive *A*–H interaction between the A cation and the H atom of the opposite O–H group (Fig. 7). Thus, the O−H group in the local OH−*A*−F configuration absorbs the IR radiation at a lower frequency than in the OH−*A*−OH configuration.

Finally, the minor absorption at 3672 cm^{-1} indicates a slight but significant departure of the composition towards tremolite (Robert *et al.*, 1989; Della Ventura and Robert, 1990; Hawthorne *et al*., 1997; Gottschalk and Andrut, 1998; Gottschalk *et al.*, 1999) and is assigned to configurations including an empty *A* site (~5%) observed in the sample.

The spectrum of endmember pargasite has been studied previously by several authors (Semet, 1973; Della Ventura *et al.*, 1999, 2003); it shows a

TABLE 6. Positions (cm^{-1}), widths (cm^{-1}) and absolute and relative intensities for the bands $A-H$ in the infrared OH-stretching spectra. The thickness of each section studied is also given. Note that a weak component around 3720 cm^{-1} is required in two samples to model the peak asymmetry on the high-frequency side of the main band. The intensity of this component is however so low it is negligible.

Band	Parameter	J9698 246 μm	C2552 174 μm	GE408 291 μm	G405 259 μm	FK1 221 μm
A′	Position		3717.3	3718.7		
	Width		15.4	15.9		
	Intensity ab.		0.44	0.79		
	Intensity re.		0.02	0.04		
A	Position	3705.6	3703.2	3706.3	3707.7	3709.1
	Width	16.2	16.3	15.9	15.9	16.8
	Intensity ab.	2.40	3.03	3.19	4.06	1.74
	Intensity re.	0.13	0.14	0.15	0.13	0.12
A*	Position	3691.3	3791.2	3693.0	3694.4	3693.6
	Width	16.3	16.3	15.9	15.9	16.8
	Intensity ab.	5.41	5.66	4.74	6.16	3.80
	Intensity re.	0.29	0.27	0.23	0.20	0.26
B	Position	3674.7	3675.4	3677.8	3680.8	3678.5
	Width	16.3	17.5	16.8	17.2	17.2
	Intensity ab.	2.89	3.72	2.67	5.28	2.61
	Intensity re.	0.15	0.18	0.13	0.17	0.18
T	Position	3671.4	3672.4	3672.8	3671.5	3671.2
	Width	9.3	9.2	9.3	9.3	9.3
	Intensity ab.	0.98	1.23	2.27	2.82	0.72
	Intensity re.	0.05	0.06	0.11	0.09	0.05
B*	Position	3658.5	3659.5	3661.8	3658.8	3659.2
	Width	16.6	17.5	16.8	17.2	17.2
	Intensity ab.	5.06	4.93	5.25	8.97	3.93
	Intensity re.	0.27	0.23	0.26	0.29	0.27
G	Position	3641.3	3641.1	3640.3	3637.8	3640.4
	Width	19.6	20.8	19.1	19.1	19.1
	Intensity ab.	1.39	1.57	1.28	2.54	1.26
	Intensity re.	0.07	0.07	0.06	0.08	0.09
H	Position	3623.0	3622.4	3624.4	3617.0	3621.4
	Width	20.1	20.7	19.4	19.4	19.4
	Intensity ab.	0.48	0.52	0.39	1.02	0.45
	Intensity re.	0.03	0.02	0.02	0.03	0.03

doublet of rather broad bands with almost equal intensity, centred at 3709 and 3678 cm^{-1}, respectively. Using the same band nomenclature, these are assigned to the local configurations MgMgMg–OH–^{A}Na:SiAl and MgMgAl–OH–^{A}Na:SiAl, respectively and derives from nearly complete Al disorder between the $M(2)$ and $M(3)$ sites (Oberti *et al.*, 1995*a*). Note that the difference in wavenumber (~30 cm^{-1}) between these two bands is due solely to the different nearest-neighbour (NN) octahedral environment ($^{M(1)}Mg^{M(1)}Mg^{M(3)}Mg$ *vs.* $^{M(1)}Mg^{M(1)}Mg^{M(3)}Al$) of the OH group, the rest of the structure in the second (T sites) and third (A site) coordination shell remaining unchanged. Note also that in pargasite, the band assigned to the vibration of the

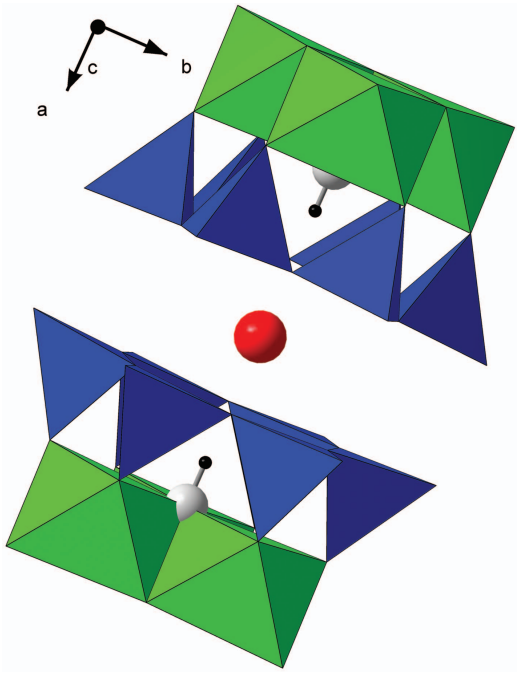

FIG. 7. A sketch of the *C*2/*m* amphibole structure showing the local environment around the O–H dipole.

O–H group bonded to a $^{M(1)}Mg^{M(1)}Mg^{M(3)}Mg$ trimer of octahedra is shifted by 20 cm^{-1} with respect to the same band in richterite; the reason for this was given by Della Ventura *et al.* (1999) and is related to the presence of Si–O(7)–Al linkages in the rings of tetrahedra in pargasite. This point will be discussed in more detail later. Similar to richterite, the presence of F at the O(3) site in pargasite shifts both the bands at 3709 and 3678 cm^{-1} (A and B, respectively, in Fig. 6, top) by 15 cm^{-1} downwards (A* and B*) and the intensity of the new bands depends on the F content (Robert *et al.*, 2000).

The spectrum of fluoro-edenite (Fig. 6, middle) is similar to that of fluoro-pargasite and its components can be assigned in a similar way. In particular, the A and B component can be assigned to the MgMgMg–OH–^{A}Na:SiAl and MgMgAl–OH–^{A}Na:SiAl configurations, while the A* and B* components can be assigned to the MgMgMg–OH/F–^{A}Na:SiAl and MgMgAl–OH/F–^{A}Na:SiAl configurations. The T component can be assigned to the tremolite-type local environment, i.e. to the presence of $^{A}\square$, in accordance with the microchemical data of Table 2. Finally, the lower-frequency bands G and H, at 3641 and 3622 cm^{-1}, respectively, are assigned to configurations involving Al occurring both as C and T cations and coupled with $^{A}\square$, i.e. to magnesio-hornblende-type configurations (Hawthorne *et al.*, 2000). Note that a weak component around 3720 cm^{-1} is required in two samples to model the peak asymmetry on the high-frequency side of the main band. The intensity of this component is low enough to be ignored in the above discussion. Final band assignments are summarized in Table 7.

In conclusion, FTIR spectra clearly show that (1) ^{C}Al in the studied samples is disordered over the *M*(2) and *M*(3) sites, thus confirming the SREF conclusions based on the analysis of the <*M*–O> bond distances; (2) similar to pargasite, the measured frequencies of all OH bands (except the minor 'tremolite'-type component at ~3672 cm^{-1}) are typical of O–H groups pointing towards Si–O(7)–Al tetrahedral linkages.

A point worth discussing here is the possible use of FTIR spectra for quantitative purposes.

TABLE 7. Final band assignments for the samples in this work. Note that in local environments involving empty *A* sites (denoted by #) the OH–OH and OH–F configurations cannot be distinguished.

Configuration				Frequency	Band
M(1)*M*(1)*M*(3)	*A*	*T*(1)*T*(1)	O(3)–O(3)	(cm^{-1})	
MgMgMg	Na	SiAl	OH–OH	3710	A, A′
MgMgMg	Na	SiAl	OH–F	3692	A*
MgMgAl	Na	SiAl	OH–OH	3678	B
MgMgAl	Na	SiAl	OH–F	3660	B*
MgMgMg	□	SiSi	OH–OH$^{\#}$	3671	T
MgMgMg	□	SiAl	OH–OH$^{\#}$	3642	G
MgMgAl	□	SiAl	OH–OH$^{\#}$	3622	H

There are several problems involved with this issue and some of these have been discussed by Hawthorne *et al.* (1996*b*, 2000). The key factors in relation to this are: (1) the obvious difficulty in using intensity data (usually band areas) obtained after a decomposition process, which might be highly subjective in the case of severe band overlap and (2) the relationship between the absorption factor (ε) and the wavenumber (ν) (e.g. Libowitzky and Rossman (1997) for hydrous minerals in general and Skogby and Rossman (1991) for amphiboles, in particular) which is still not completely understood (Della Ventura *et al*., 1996, Hawthorne *et al*., 1996*b*). Due to these problems, the measured intensities cannot be converted accurately to site populations. For the present case, the site populations derived from the spectral decomposition and band assignment must be in accord with the data derived by SREF on the same samples. If this is the case, the band parameters such as the band width can be constrained confidently to appropriate values and then compared with the data known from the refinement of synthetic samples (e.g. Della Ventura *et al.*, 1999). We can test the band-fitting model described above by calculating the OH/F composition and the amount of A cations from the intensity data in Table 6. For the OH/F ratio the relationship $I_A+I_B/(I_A+I_{A*}+I_B+I_{B*})$ (Robert *et al.*, 2000) was used, while for the A cations the equation $x = R/[k+R(1-k)]$ (Hawthorne *et al.*, 1997) was used, where x is the tremolite component in the amphibole, R is the relative intensity ratio between A site-vacant and A site-occupied OH-bands and k is 2.2. The results given in Table 8 show a good agreement between FTIR- and EMPA-derived site populations and suggest that both the band assignment and the fitting model are adequate, at least for well characterized and sufficiently chemically simple amphiboles.

Short-range order of ^{T}Al in fluoro-edenite and fluoro-pargasite

The knowledge of Al partitioning in amphiboles has important implications for the geobarometry of igneous and metamorphic processes (e.g. Spear, 1981; Hammarstrom and Zen, 1986; Hollister *et al.*, 1987; Ridolfi *et al*., 2010). Most thermodynamic analyses (e.g. Graham and Navrotsky, 1986) have so far considered activity models based solely on the occurrence of ^{C}Al at $M(2)$ and ^{T}Al at $T(1)$. Crystal-chemical work has shown that these mixing models are inadequate, at least in pargasite, where ^{C}Al can disorder between the $M(2)$ and $M(3)$ sites in Mg-rich compositions crystallized at high T (e.g. Oberti *et al*., 1995*a*) and ^{T}Al can either occupy the $T(2)$ site at ^{T}Al > 2.0 a.p.f.u. or disorder between the $T(1)$ and $T(2)$ sites at high temperature (Oberti *et al.*, 1995*b*). Long-range ordering (LRO) patterns of Al in amphiboles are now understood quite well (see Oberti *et al.* (2007) for a complete discussion of modern data), but we still know very little about the short-range order of Al. The X-ray scattering factors for Al and Si are very similar, therefore X-ray diffraction can provide long-range information on the ordering pattern of T cations based solely on the analysis of the mean $<T(1)-O>$ and $<T(2)-O>$ bond distances. When applied to amphiboles, the bond-valence theory (Brown, 1981, 2002) showed systematically that cation ordering patterns are strongly constrained by the bond-strength requirements of the coordinated oxygen atoms (Hawthorne, 1997). One resulting and fundamental feature, in amphibole crystal-chemistry is the avoidance of Al−O−Al linkages in the double chain of tetrahedra. Attempts to understand both long-range and short-range order via ^{29}Si MAS NMR (magic-angle spinning nuclear magnetic resonance), which is sensitive to NN and NNN (next nearest neighbour)

TABLE 8. Comparison between the FTIR- and EMPA-derived ^{W}F and $^{A}\square$ contents for the samples studied.

Sample	^{W}F FTIR	^{W}F EMPA	$^{A}\square$ FTIR	$^{A}\square$ EMPA
J9698	1.36	1.41	0.07	0.08
C2552	1.22	1.31	0.07	0.07
Ge408	1.28	1.14	0.10	0.21
G405	1.24	1.46	0.10	0.09
FK1	1.28	1.18	0.08	0.12

environments around the target Si nuclei, have been carried out by Welch *et al.*, (1994, 1998). However, the ^{29}Si MAS NMR results are still relatively difficult to interpret and model.

A deeper insight into this problem can be obtained by considering the stereochemistry of the *T* sites in Al-bearing amphiboles and by close comparison of the OH-spectra of fluoro-edenite with endmembers richterite and pargasite (Fig. 8).

Structure refinement results for the fluoro-edenite and fluoro-pargasite samples used in this work, indicate that ^{T}Al is completely ordered at *T*(1). As stated above, the higher-frequency component in the spectrum of pargasite is assigned to the same NN configuration of

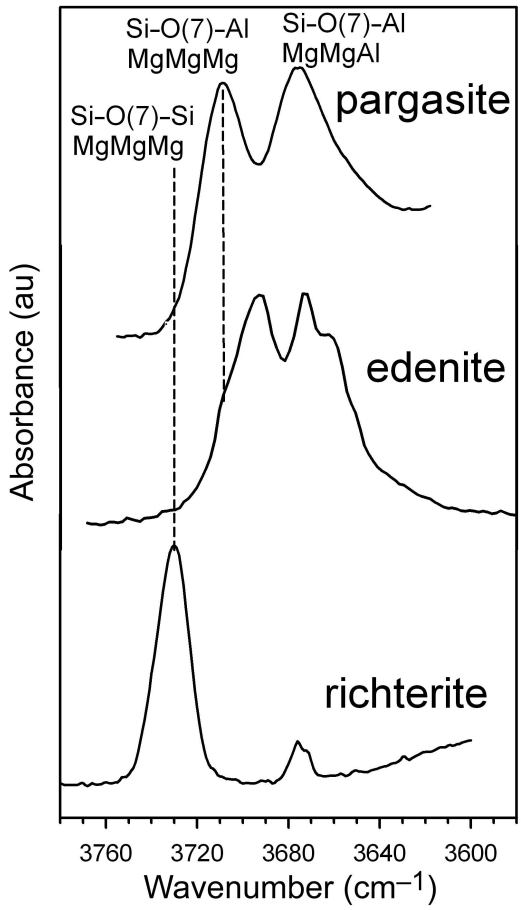

FIG. 8. The OH-stretching spectra of synthetic pargasite (from Della Ventura *et al*., 1999), fluoro-edenite from Franklin (sample C2552, this work) and synthetic richterite (from Robert *et al*., 1989). The local configurations are schematically given in the figure.

richterite, i.e. $M(1)M(1)M(3)-O(3)-A$ = MgMgMg−OH−^{A}Na. The observed shift in pargasite toward a lower frequency with respect to richterite (3709 cm^{-1} *vs*. 3730 cm^{-1}, Raudsepp *et al.*, 1987, Della Ventura *et al.*, 1999, 2001) is an important feature in the FTIR spectroscopy of the amphiboles (and any hydroxyl-bearing silicate). This has been explained by a H bond to the O(7) oxygen atom (Fig. 9), the strength of the bond controlling the shift in the frequency of the principal OH-stretching vibration (Della Ventura *et al.*, 1999, 2003; Libowitzky and Beran, 2004). The key issue here is that the valence-sum rule must be satisfied at the O(7) anion, which is bonded solely to two *T*(1) tetrahedra (Fig. 9). When the *T*(1)−O(7)−*T*(1) linkages are of the type Si−O(7)−Al, the deficit in bond valence at the O(7) anion must be alleviated *via* a stronger O(3)−H···O(7) bonding. Hence we can use the spectra of Figs 1 and 2 to evaluate the SRO of cations at the *T*(1) sites in the studied amphiboles.

Consider the double-chain of tetrahedra in richterite (Fig. 10*a*). All the tetrahedra are occupied by Si and hence all *T*(1)−O(7)−*T*(1) linkages are of the Si−O(7)−Si type. Therefore, we observe a unique OH-stretching band at 3730 cm^{-1}. Consider next the double-chain of tetrahedra in stoichiometric pargasite (Fig. 10*b*). The composition of the double chain of tetrahedra is Si_6Al_2; hence, the *T*(2) sites are occupied by Si and half of the *T*(1) sites are occupied by Al. All the *T*(1)−O(7)−*T*(1) linkages must be of the Si−O(7)−Al type to avoid Al−O−Al linkages (cf. the Löwenstein rule; Löwenstein, 1954). In such a case, all the H atoms are involved in H bonding with the closest O(7) atom and all the OH-stretching bands are displaced by 20 cm^{-1} toward lower frequencies. In particular, the MgMgMg−OH−^{A}Na:SiAl band is found at 3709 cm^{-1}. In local configurations where ^{C}Al occurs at the NN *M* sites, i.e. the MgMgAl−OH−^{A}Na:SiAl configurations, the band has an additional shift of ~30 cm^{-1}, i.e. at 3675 cm^{-1} with respect to the corresponding band in richterite (band B in Fig. 6).

Now consider fluoro-edenite. In stoichiometric edenite, the composition of the double chain of tetrahedra is Si_7Al_1 hence half of *T*(1)−O(7)−*T*(1) linkages must be of the Si−O(7)−Si type and half must be of the Si−O(7)−Al type; in such a case, there are at least two possible patterns of order between $^{T(1)}$Si and $^{T(1)}$Al and these must have different spectral expressions in the infrared region. Figure 10*c* shows the most ordered

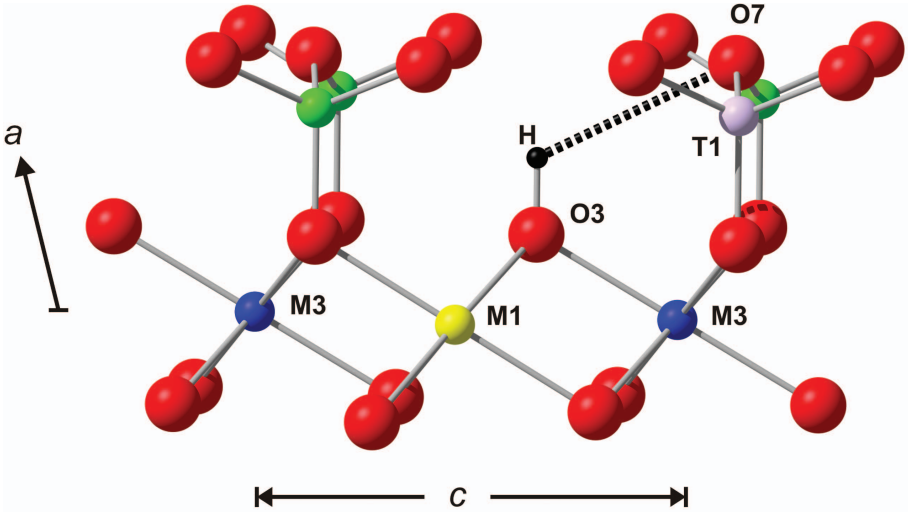

FIG. 9. The local environment of the H atom in the *C*2/*m* amphibole structure viewed down [010]; the *T*(2) sites have been omitted for clarity. Green = Si, grey = Al. Modified from Della Ventura *et al*. (1999).

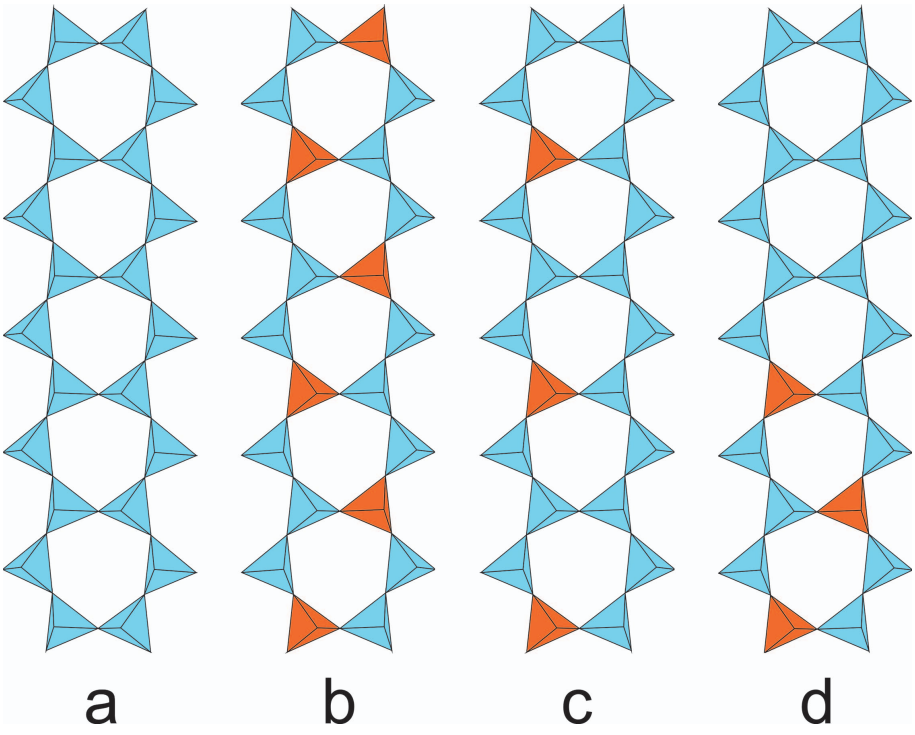

FIG. 10. Schematic tetrahedral chain arrangements in (*a*) richterite; (*b*) pargasite; (*c*) edenite, regularly alternated; (*d*) edenite, clustered. For more explanation, see text. Blue tetrahedra = Si, orange tetrahedra = Al. Note that when the *T*(1)–O(7)–*T*(1) linkages have the configuration Al–O(7)–Si there can be orientational disorder relative to the *b* direction.

pattern, with Si−O(7)−Si linkages regularly alternating with Si−O(7)−Al linkages. Figure 10*d* shows another 'ordered' possibility, where clusters of Si−O(7)−Al linkages alternate with clusters of Si−O(7)−Si linkages (the number of the linkages in the two clusters being equal).

In the first model, all the OH-stretching bands must be of the pargasite-type and fall at ~3709 cm^{-1} (or at a lower wavenumber if cations other than Mg occur at the *M*(1,3) sites, e.g. Della Ventura *et al*., 1996). In the second model, we should observe two bands with almost the same intensity occurring at 3730 and 3709 cm^{-1} (again, if the C cation composition is Mg_5). The systematic lack of a band at 3730 cm^{-1} in the spectrum of the studied fluoro-edenite and fluoro-pargasite samples of this work (Figs 1,2) shows that this is not the case. Hence, the double chain of tetrahedra in fluoro-edenite has the short range ordered configuration schematically shown in Fig. 10*c*.

Acknowledgements

Marcello Serracino assisted during the EMP analyses and Antonio Gianfagna supported the EMP analyses financially. Thanks are due to Dr Pete J. Dunn, Smithsonian Institution, National Museum of Natural History and Dr John Cianciulli, Franklin Mineral Museum for providing the samples studied. Roberta Oberti acknowledges funding from the MIUR-PRIN 2009 project 'Structure, microstructures and cation ordering: a window on to geological processes and geomaterial properties'. Thanks are due to S. Mills, D. Jenkins and a further anonymous referee for their helpful suggestions.

References

Brown, I.D. (1981) The bond-valence method: an empirical approach to chemical structure and bonding. Pp. 1−30 in: *Structure and bonding in crystals* (M. O'Keeffe and A. Navrotsky, editors), vol. **2**, Academic Press, New York, USA.

Brown, I.D. (2002) *The Chemical Bond in Inorganic Chemistry: the Bond-valence Model*. Oxford University Press, Oxford, UK, 278 pp.

Boschmann, K.F., Burns, P.C., Hawthorne, F.C., Raudsepp, M. and Turnock, A.C. (1994) A-site disorder in synthetic fuor-edenite, a crystal-structure study. *The Canadian Mineralogist*, **32**, 21−30.

Cámara, F. (1995) *Estudio cristalquímico de minerales metamórficos en rocas básicas del Complejo Nevado-Filábride (Cordilleras Béticas)*. PhD thesis, University of Granada, 484 pp. [In Spanish].

Clark, A.M. (1993) *Hey's Mineral Index: Mineral Species, Varieties and Synonyms*. Chapman & Hall, London.

Della Ventura, G. (1992) Recent developments in the synthesis and characterization of amphiboles. Synthesis and crystal-chemistry of richterites. *Trends in Mineralogy*, **1**, 153−192.

Della Ventura, G. and Robert, J.-L. (1990) Synthesis, XRD and FT-IR studies of strontium richterites. *European Journal of Mineralogy*, **2**, 171−175.

Della Ventura, G., Robert, J.L. and Hawthorne, F.C. (1996) Infrared spectroscopy of synthetic (Ni,Mg,Co)-potassium-richterite. Pp. 55−63 in *Mineral Spectroscopy: a Tribute to Roger G. Burns* (M.D. Dyar, C. McCammon and M.W. Schaefer, editors). The Geochemical Society Special Publication, **5**. St Louis, Missouri, USA.

Della Ventura, G., Hawthorne, F.C., Robert, J.-L., Delbove, F., Welch, M.D. and Raudsepp, M. (1999) Short-range order of cations in synthetic amphiboles along the richterite-pargasite join. *European Journal of Mineralogy*, **11**, 79−94.

Della Ventura, G., Robert, J.-L., Sergent, J., Hawthorne, F.C. and Delbove, F. (2001) Constraints on F vs. OH incorporation in synthetic $^{[6]}$Al-bearing monoclinic amphiboles. *European Journal of Mineralogy*, **13**, 841−847.

Della Ventura, G., Hawthorne, F.C., Robert, J.-L. and Iezzi, G. (2003) Synthesis and infrared spectroscopy of amphiboles along the tremolite-pargasite join. *European Journal of Mineralogy*, **15**, 341−347.

Farmer, V.C. (editor) (1974) *The Infrared Spectra of Minerals*. Mineralogical Society Monograph **4**. The Mineralogical Society, London.

Gianfagna, A. and Oberti, R. (2001) Fluoro-edenite from Biancavilla (Catania, Sicily, Italy): crystal chemistry of a new amphibole end-member. *American Mineralogist*, **86**, 1489−1493.

Gilbert, M.C., Helz, R.T., Popp, R.K. and Spear, F.S. (1982) Experimental studies on amphibole stability. Pp. 229−353 in: *Amphiboles: Petrology and Experimental Phase Relations* (D.R. Veblen and P.H Ribbe, editors). Reviews in Mineralogy, **9B**. Mineralogical Society of America, Washington DC, USA.

Gottschalk, M. and Andrut, M. (1998) Structural and chemical characterization of synthetic (Na,K)-richterite solid solution by EMP, HRTEM, XRD and OH-valence spectroscopy. *Physics and Chemistry of Minerals*, **25**, 101−111.

Gottschalk, M., Andrut, M. and Melzer, S. (1999) The determination of the cummingtonite content of synthetic tremolite. *European Journal of Mineralogy*, **11**, 967−982.

Graham, C.M. and Navrotsky, A. (1986) Thermochemistry of the tremolite-edenite amphiboles using fluorine anlogues and applications to amphibole-plagioclase-quartz equilibria. *Contributions to Mineralogy and Petrology*, **93**, 18–32.

Hammarstrom, J.M. and Zen, E-an (1986) Aluminum in hornblende: an empirical igneous geobarometer. *American Mineralogist*, **71**, 1297–1313.

Hawthorne, F.C., Oberti, R. and Sardone, N. (1996*a*) Sodium at the A site in clinoamphiboles: the effects of composition on patterns of order. *The Canadian Mineralogist*, **34**, 577–593.

Hawthorne, F.C., Della Ventura, G. and Robert, J.L. (1996*b*) Short-range order and long-range order in amphiboles: a model for the interpretation of infrared spectra in the principal OH-stretching region. Pp. 49–54 in: *Mineral Spectroscopy: a Tribute to Roger G. Burns* (M.D. Dyar, C. McCammon and M.W. Schaefer, editors). The Geochemical Society Special Publication, **5**. St Louis, Missouri, USA.

Hawthorne, F.C. (1997) Short-range order in amphiboles: a bond-valence approach. *The Canadian Mineralogist*, **35**, 201–216.

Hawthorne, F.C., Della Ventura, G., Robert, J.-L., Welch, M.D., Raudsepp, M. and Jenkins, D.M. (1997) A Rietveld and infrared study of synthetic amphiboles along the potassium-richterite-tremolite join. *American Mineralogist*, **82**, 708–716.

Hawthorne, F.C., Welch, M.D., Della Ventura, G., Liu, S., Robert, J.-L. and Jenkins, D.M. (2000) Short-range order in synthetic aluminous tremolites: an infrared and triple quantum MAS NMR study. *American Mineralogist*, **85**, 1716–1724.

Hawthorne, F.C. and Della Ventura, G. (2007) Short-range order in amphiboles Pp. 173–222 in: *Amphiboles: Crystal-chemistry, Occurrence and Health Issues* (F.C. Hawthorne, R. Oberti, G. Della Ventura and A. Mottana, editors). Reviews in Mineralogy and Geochemistry, **67**. Mineralogical Society of America and the Geochemical Society, Washington, D.C.

Hawthorne, F.C., Oberti, R., Harlow, G.E., Maresch, W.V., Martin, R.F., Shumacher, J.C. and Welch, M.D. (2012) IMA report. Nomenclature of the amphibole supergroup. *American Mineralogist*, **97**, 2031–2048.

Hollister, L.S., Grissom, G.C., Peters, E.K., Stowell, H.H. and Sisson, V.B. (1987) Confirmation of the empirical correlation of Al in hornblende with pressure of solidification of calc-alkaline plutons. *American Mineralogist*, **72**, 231–239.

Kohn, J.A. and Comeforo, J.E. (1955) Synthetic asbestos investigations. II. X-ray and other data on synthetic fluor-richterite, -edenite and boron-edenite. *American Mineralogist*, **40**, 410–421.

Koch-Müller M., Matsyuk S.S. and Wirth R. (2004) Hydroxyl in omphacites and omphacitic clinopyroxenes of upper mantle to lower crustal origin beneath the Siberian platform. *American Mineralogist*, **89**, 921–931.

Libowitzky, E. and Rossman, G.R. (1997) An IR absorption calibration for water in minerals. *American Mineralogist*, **82**, 1111–1115.

Libowitzky, E. and Beran, A. (2004) IR spectroscopy as a tool for the characterization of hydrous species in minerals. Pp. 227–280 in: *Spectroscopic Methods in Mineralogy* (A. Beran and E. Libowitzky, editors). EMU Notes in Mineralogy, **6**. European Mineralogical Union, Eötvös University Press, Budapest.

Löwenstein, W. (1954) The distribution of aluminum in the tetrahedra of silicates and aluminosilicates. *American Mineralogist*, **39**, 92–96.

Na, K.C., McCauley, M.L., Crisp, J.A. and Ernst, W.G. (1986) Phase relations to 3 kbar in the system edenite + H_2O and edenite + excess quartz + H_2O. *Lithos*, **19**, 153–163.

Oberti, R., Hawthorne, F.C., Ungaretti, L. and Cannillo, E. (1995*a*) $^{[6]}$Al disorder in amphiboles from mantle peridotites. *The Canadian Mineralogist*, **33**, 867–878.

Oberti, R., Ungaretti, L., Cannillo, E., Hawthorne, F.C. and Memmi, I. (1995*b*) Temperature-dependent Al order-disorder in the tetrahedral double-chain of *C*2/*m* amphiboles. *European Journal of Mineralogy*, **7**, 1049–1063.

Oberti, R., Hawthorne, F.C. and Raudsepp, M. (1997) The behaviour of Mn in amphiboles: Mn in synthetic fluoro-edenite and synthetic fluoropargasite. *European Journal of Mineralogy*, **9**, 115–122.

Oberti, R., Cámara, F., Della Ventura, G., Iezzi, G. and Benimoff, A.I. (2006) Parvo-mangano-edenite and parvo-manganotremolite, two new Group 5 monoclinic amphiboles from Fowler, New York and comments on the solid solution between Ca and Mn^{2+} at the M(4) site. *American Mineralogist*, **91**, 526–532.

Oberti, R., Hawthorne, F.C., Cannillo, E. and Cámara, F. (2007) Long-range order in amphiboles. Pp. 125–171 in: *Amphiboles: Crystal-chemistry, Occurrence and Health Issues* (F.C. Hawthorne, R.Oberti, G. Della Ventura and A. Mottana, editors). Reviews in Mineralogy and Geochemistry, **67**. Mineralogical Society of America and the Geochemical Society, Washington, D.C.

Palache, C. (1935) *The minerals of Franklin and Sterling Hill, Sussex County, New Jersey*. United States Geological Survey Professional Paper **180**, 135 pp.

Pouchou, J.L. and Pichoir, F. (1985) 'PAP' $\Phi(\rho Z)$ procedure for improved quantitative micro-analysis.

Microbeam Analysis, **1985**, 104–160.

Raudsepp, M., Turnock, A.C., Hawthorne, F.C., Sherriff, B.L. and Hartman, J.S. (1987): Characterization of synthetic pargasitic amphiboles [$NaCa_2Mg_4M^{3+}Si_6Al_2O_{22}(OH,F)_2$; M^{3+} = Al, Cr, Ga, Sc, In] by infrared spectroscopy, Rietveld structure refinement and ^{27}Al, ^{29}Si and ^{19}F MAS NMR spectroscopy. *American Mineralogist*, **72**, 580–593.

Raudsepp, M., Turnock, A.C. and Hawthorne, F.C. (1991) Amphibole synthesis at low pressure: what grows and what doesn't. *European Journal of Mineralogy*, **3**, 983–1004.

Ridolfi, F., Renzulli, A. and Puerini, M. (2010) Stability and chemical equilibrium of amphibole in calc-alkaline magmas: an overview, new thermobarometric formulations and application to subduction-related volcanoes. *Contributions to Mineralogy and Petrology*, **160**, 45–66.

Robert, J.-L., Della Ventura, G. and Thauvin, J.-L. (1989) The infrared OH-stretching region of synthetic richterites in the system Na_2O–K_2O–CaO–MgO–SiO_2–H_2O–HF. *European Journal of Mineralogy*, **1**, 203–211.

Robert, J.-L., Della Ventura, G. and Hawthorne, F.C. (1999) Near-infrared study of short-range disorder of OH and F in monoclinic amphiboles. *American Mineralogist*, **84**, 86–91.

Robert, J.-L., Della Ventura, G., Welch, M. and Hawthorne, F.C. (2000) OH-F substitution in synthetic pargasite at 1.5 kbar, 850ºC. *American Mineralogist*, **85**, 926–931.

Semet, M.P. (1973) A crystal-chemical study of synthetic magnesiohastingsite. *American Mineralogist*, **58**, 480–494.

Skogby, H. and Rossman, G.R. (1991) The intensity of amphibole OH bands in the infrared absorption spectrum. *Physics and Chemistry of Minerals*, **18**, 64–68.

Soto, J.I. (1991) *Estructura y evolución metamórfica del Complejo Nevado-Filábride en la terminación oriental de la Sierra de los Filabres (Cordilleras Béticas)*. PhD Thesis, University of Granada, 273 pp.

Spear, F.S. (1981) An experimental study of hornblende stability and compositional variability in amphibolite. *American Journal of Science*, **281**, 697–734.

Strens, R.S.J. (1974) The common chain, ribbon and ring silicates. Pp 305–330 in: *The Infrared Spectra of Minerals* (V.C. Farmer, editor). Mineralogical Society Monograph, **4**. The Mineralogical Society, London.

Welch, M.D., Kolodziejski, W. and Klinowski, J. (1994) A multinuclear NMR study of synthetic pargasite. *American Mineralogist*, **79**, 261–268.

Welch, M.D., Liu, S. and Klinowski, J. (1998) ^{29}Si MAS NMR systematics of calcic and sodic-calcic amphiboles. *American Mineralogist*, **83**, 85–96.